Alternative Splicing of the β_4 Subunit Has α_1 Subunit Subtype-Specific Effects on Ca^{2+} Channel Gating

Thomas D. Helton and William A. Horne

Department of Anatomy, Physiological Sciences, and Radiology, North Carolina State University College of Veterinary Medicine, Raleigh, North Carolina 27606

Ca^{2+} channel β subunits are important molecular determinants of the kinetics and voltage dependence of Ca^{2+} channel gating. Through direct interactions with channel-forming α_1 subunits, β subunits enhance expression levels, accelerate activation, and have variable effects on inactivation. Four distinct β subunit genes each encode five homologous sequence domains (D1–5), three of which (D1, D3, and D5) undergo alternative splicing. We have isolated from human spinal cord a novel alternatively spliced β_4 subunit containing a short form of domain D1 (β_{4a}) that is highly homologous to N termini of *Xenopus* and rat β_3 subunits. The purpose of this study was to compare the gating properties of various α_1 subunit complexes containing β_{4a} with those of complexes containing a β_4 subunit with a longer form of domain D1, β_{4b}. Expression in *Xenopus* oocytes revealed that, relative to α_{1A} and α_{1B} complexes containing β_{4b}, the voltage dependence of activation and inactivation of complexes containing β_{4a} were shifted to more depolarized potentials. Moreover, α_{1A} and α_{1B} complexes containing β_{4a} inactivated at a faster rate. Interestingly, β_4 subunit alternative splicing did not influence the gating properties of α_{1C} and α_{1E} subunits. Experiments with β_4 deletion mutants revealed that both the N and C termini of the β_4 subunit play critical roles in setting voltage-dependent gating parameters and that their effects are α_1 subunit specific. Our data are best explained by a model in which distinct modes of activation and inactivation result from β-subunit splice variant-specific interactions with an α_1 subunit gating structure.

Key words: β4 subunit; alternative splicing; N terminus; calcium channel; gating; voltage clamp; spinal cord

Neuronal high voltage-activated Ca^{2+} channels (L, N, P/Q, and R) consist of at least four subunits, α_1, α_2/δ, and β (Liu et al., 1996), with a fifth subunit, γ, being recently described (Letts et al., 1998). Different Ca^{2+} channel phenotypes arise primarily from the expression of five unique α_1 subunit genes (α_{1A}–α_{1E}). These genes encode large pore-forming proteins (>2200 amino acids) that are differentially distributed throughout the nervous system (Westenbroek et al., 1990, 1998). Synaptic N-, P/Q-, and R-type channels, formed by α_{1B}, α_{1A}, and α_{1E} subunits, respectively, play a principal role in regulating neurotransmitter release (Turner et al., 1992; Takahashi and Momiyama, 1993; Wheeler et al., 1994; Wu et al., 1999).

Ca^{2+} channel β subunits (subtypes 1–4) are highly homologous intracellular proteins with primary sequences ranging from 480 to 630 amino acids (for review, see Birnbaumer et al., 1998). The sequence can be divided into five domains on the basis of the regions of amino acid identity between subtypes. All β subunits contain a highly conserved β interaction domain (BID) in domain 4, which has been shown to interact with high affinity to an α interaction domain (AID) on the I–II linker of α_1 subunits (Pragnell et al., 1994; De Waard and Campbell, 1995). Structure prediction methods using the Prodom and Pfam protein databases have established a domain structure (A–E domains) for the β_{1b} subunit (Hanlon et al., 1999) that primarily overlaps with sequence domains 1–5. The A domain [100 amino acids (aa)] shows some homology to PDZ domains, the B domain (61 aa) to SH3 domains, and the D domain (210 aa) to guanylate-kinase, although it lacks a functional ATP-binding P-loop motif. Domains C and E were without precedent in the Prodom and Pfam protein databases; however, Domain C is rich in serine residues, suggesting that it serves a linker function between domains B and D. Thus, in many respects, Ca^{2+} channel β subunits resemble members of the membrane-associated guanylate kinase (MAGUK) protein family, which are known to cluster ion channels, receptors, adhesion molecules, and cytosolic signaling proteins at synapses and cellular junctions (Fanning and Anderson, 1999).

Previous studies have shown that the kinetics and voltage sensitivity of α_1 subunit gating are affected profoundly by β subunits (Lacerda et al., 1991; Singer et al., 1991), and the extent to which these parameters are altered varies significantly with β subunit subtype (Ellinor et al., 1993; Olcese et al., 1994). For example, although β_1 and β_3 subunits shift the voltage dependence of α_{1E} subunit inactivation to more hyperpolarized potentials, β_2 subunits have a marked depolarizing effect (for review, see Birnbaumer et al., 1998). Moreover, the responsiveness of α_1 subunits to β subunit modulation can be modified by alternative splicing of both β (Olcese et al., 1994; Qin et al., 1996) and α_1 subunits (Krovetz et al., 2000; Pan and Lipscombe, 2000). In this study, we demonstrate for the first time that alternative splicing of the N terminus of the β_4 subunit alters Ca^{2+} channel gating and that this effect is specific to α_{1A} and α_{1B} subunits.

Received June 29, 2001; revised Dec. 5, 2001; accepted Dec. 7, 2001.

This work was supported by National Institutes of Health Grant R29-NS 32094, North Carolina Biotechnology Center Academic Research Grant 9905 ARG 0044, and a College of Veterinary Medicine State Research Support Grant. We thank Dr. Robert Rosenberg for advice on data analysis and manuscript preparation.

Correspondence should be addressed to Dr. William A. Horne, Department of Anatomy, Physiological Sciences, and Radiology, North Carolina State University College of Veterinary Medicine, 4700 Hillsborough Street, Raleigh, NC 27606. E-mail: bill_horne@ncsu.edu.

 0270-6474/02/221573-10$15.00/0

MATERIALS AND METHODS

Human spinal cord library screening. Calcium channel β_4 subunits were isolated from an oligo-dT and random-primed human spinal cord λgt11 5′-Stretch Plus cDNA library (Clontech, Palo Alto, CA) using a nonradioactive digoxigenin-labeling and colorimetric detection system (Roche Molecular Biochemicals, Indianapolis, IN). The library was constructed from mRNA isolated from whole spinal cords pooled from 26 male and female Caucasians, ages 16–75 years, who died of sudden death syndrome. The insert size range of the library was 0.8–7.0 kb (average size 1.7 kb). Plaque-purified phage DNAs were isolated using a Lambda Prep Kit (Qiagen, Santa Clara, CA) and digested with the restriction endonuclease *Eco*RI (all endonucleases used were from Roche Molecular Biochemicals). All cDNA isolates were ligated into pBluescriptII (Stratagene, La Jolla, CA) for PCR-based cycle sequencing (FS chemistry; PE Biosystems, Foster City, CA) with universal and custom internal primers (Genosys, The Woodlands, TX). Sequences were obtained using an ABI Prism 310 Genetic DNA analyzer, and data were analyzed using ABI Prism DNA Sequencing Software (Version 2.12; PE Biosystems). Sequence comparisons, alignments, and restriction maps were performed using Lasergene Software (DNA Star, Madison, WI).

The library-screening process was initiated with a human brain β_4 cDNA probe obtained from the National Center for Biotechnical Information dbEST database (1.5 kb human fetal brain β_4 fragment; GenBank number R15035). Of nine first-round β_4 cDNAs isolated, the 1.6 kb β_4-7 clone was the largest, extending from nucleotide 216 to beyond an in-frame stop codon (the human brain β_4 cDNA, GenBank number U95020, was used as a reference for all β_4 nucleotide and amino acid positions). The β_4-7 clone contained 134 nucleotides of 5′ untranslated sequence. A second round of screening, using a probe consisting of the N-terminal portion of β_4-7 from an internal *Bam*HI site (550) to the 5′ untranslated region, yielded seven additional β_4 cDNAs, β_4-15 to β_4-22. Clone β_4-17 possessed an in-frame start codon and novel exon 1 sequence but lacked the last 33 nucleotides of the human brain β_4 C-terminal coding sequence. Therefore, to create a full-length β_4 cDNA, the N terminus of the β_4-17 clone from the *Bam*HI site at nucleotide position 550 to the *Bam*HI site in the pBluescript II was ligated into a *Bam*HI-prepared β_4-7 clone. Sequence analysis was used to confirm that the β_4-17/7 ligation occurred in the proper orientation. This full-length β_4 cDNA was referred to as β_{4a} (GenBank number AY054985). We used RT-PCR to isolate the previously published human brain β_4 N terminus (U95020). A 694 bp fragment was obtained using a commercially available RT-PCR kit (Stratagene), custom oligonucleotide primers (β_4 25F: 5′-CTCCGCCCACCGCACACG; β_4 719R: 5′-CTAACACCACCGGACGCAT), and human spinal cord poly(A^+) RNA (Clontech). Complete sequence analysis determined that the 694 bp fragment was identical to the U95020 N terminus, that it contained a start codon, and that it extended beyond the *Bam*HI restriction site at position 550. Therefore, to make a second full-length β_4 subunit, this fragment was cloned into a *Bam*HI-prepared pBluescriptII SK+ vector containing β_4-7. Sequence analysis was used to confirm correct reading frame and proper N-terminal orientation. This full-length β_4 cDNA was referred to as β_{4b}.

Construction of $\beta_4\Delta N$, $\beta_{4a}\Delta C$, $\beta_{4b}\Delta C$, and $\beta_4\Delta N/\Delta C$ deletion mutants. A β_4 cDNA lacking exon 1 ($\beta_4\Delta N$) was obtained by using PCR to replace exon 1 of β_{4a} with an idealized Kozak sequence (Kozak, 1991) and start codon. Custom oligonucleotide primers $\beta_4\Delta NF$ (5′-GCCACCATGGGTTCAGCGGATTCC), containing the Kozak sequence and start codon and beginning at nucleotide 215, and β_4 719R were used in a PCR reaction with the β_4-17 clone as template to generate the fragment, $\beta_4NT(-)$. This fragment was then cloned into the *Bam*HI-prepared β_4-7 cDNA and sequenced to confirm correct reading frame and proper N-terminal orientation. The $\beta_{4a}\Delta C$, $\beta_{4b}\Delta C$, and $\beta_4\Delta N/\Delta C$ cDNAs were obtained by using PCR to remove the C-terminal nucleotide sequence 3′ to nucleotide 1286 (corresponding to amino acid position 404). Custom oligonucleotide primers β_4 849F (5′-GCTGACATTTCTCTTGCTAA upstream of a unique *Bgl*II site) and $\beta_4\Delta CR$ (5′-TCAGGTTGTGTGGGTGGCAC, which ended at β_4 nucleotide 1286 and included an in-frame stop codon) were used in a PCR reaction with the β_4-17 clone as template to generate the truncated fragment, $\beta_4C(-)$. This fragment was then cloned into the pT-Advantage vector (Clontech) and sequenced to determine correct orientation. The $\beta_4C(-)$ fragment was then cut with *Bgl*II and *Xho*I (from pT-Advantage poly-linker) and cloned into *Bgl*II- and *Xho*I-prepared β_{4a}, β_{4b}, and $\beta_4\Delta N$ cDNAs. The resulting cDNAs were then sequenced with internal primers flanking the C-terminal deletion to confirm sequence orientation and fidelity.

The BI-2 (α_{1A}) and α_{2a}/δ-1 clones used in this study were provided by T. Tanabe (Tokyo Medical and Dental University, Tokyo, Japan). The rat α_{1B} and rabbit α_{1C} clones were kindly provided by D. Lipscombe (Brown University, Providence, RI) and E. Perez-Reyes (University of Virginia, Charlottesville, VA), respectively.

Electrophysiology and data analysis. Complementary RNAs (cRNAs) were synthesized *in vitro* using Ambion's mMessage mMachine RNA transcription kit [T3 or T7 depending on clone orientation in pBluescript II S/K^+ or pBSTA (α_{1B})]. Standard *Xenopus laevis* oocyte expression methods were used to characterize β subunit splice variants. Briefly, full-length α_1, α_2/δ, and β cRNAs were injected in equimolar ratios (5.6 ng $\alpha_{1A\ or}\ \alpha_{1B}$, 2.4 ng α_2/δ, and 1.6 ng β in 46 nl; 17 ng α_{1C} or α_{1E}, 7 ng α_2/δ, and 5 ng β in 50 nl) into defolliculated oocytes (stage V–VI). (The $\alpha_2\delta$-1 subunit was used in this study.) Calcium channel currents were recorded 2–8 d after oocyte injection by standard two-electrode voltage clamp using a Warner amplifier (OC-725B) at 20–22°C, and data were collected using pCLAMP6 software (Axon Instruments, Foster City, CA). Microelectrodes were filled with 3 M KCl, and the resistances of the current and voltage electrodes were 0.3–1.5 MΩ. Data were filtered at 2 kHz and sampled at 10 kHz. Currents were recorded in a chloride-free bath containing 5 mM $Ba(OH)_2$, 5 mM HEPES, 85 mM TEA-OH, and 2 mM KOH, pH adjusted to 7.4 with methansulfonic acid (α_{1A} and α_{1B}), or 40 mM $Ba(OH)_2$, 5 mM HEPES, 85 mM TEA-OH, and 2 mM KOH, pH adjusted to 7.4 with methansulfonic acid (α_{1C} and α_{1E}). Currents used to generate the data in this study ranged from 0.5 to 2.9 μA. For activation and inactivation experiments, the average current sizes for α_{1A} and α_{1B} complexes containing either β_{4a} or β_{4b} were 1.2 and 1.6 μA, respectively. Leak currents were between 20 and 100 nA. Only recordings with minimal tail currents were used for each data set (see representative traces in Fig. 5). Data were analyzed using pCLAMP6 software (Axon Instruments) and Excel 7.0 (Microsoft Corp., Redmond WA). The leak and capacitive currents were subtracted on-line using a standard P/4 protocol. Boltzmann fits to the activation and inactivation data were performed using Sigma Plot version 5.0 (SSPS Inc., Chicago IL) with the equations $\%I_{Ba} = 1/[1 + \exp(-(V_{test} - V_{1/2})/k)]$ and $\%I_{Ba} = 1/[1 + \exp((V_{pre} - V_{1/2})/k)]$, respectively, where $V_{test} = I$–V test potential, V_{pre} = prepulse potential, $V_{1/2}$ = midpoint of activation or inactivation, and k = slope factor. An estimate of gating charge, z, was calculated by dividing 25 (approximate value for RT/F at room temperature, where R = gas constant, T = temperature, and F = Faraday constant) by the slope factor. Statistical analysis was performed with a Student's two-sample equal variance t test with a two-tailed distribution (Microsoft Excel 97 SR-2). Data are presented as mean ± SEM.

RESULTS

Cloning of a Ca^{2+} channel β_4 subunit with an N terminus similar to that of β_3 subunits

Two β_4 subunit N-terminal splice variants, β_{4a} and β_{4b} (Fig. 1), are the focus of this study. Both were isolated from a human spinal cord cDNA library using routine screening techniques. The amino acid sequence of the β_{4b} variant is identical to a previously published sequence (GenBank number U95020), whereas this is the first reporting of the β_{4a} sequence. The difference in the two variants lies solely in the nucleotide sequence of exon 1, the translated region of which is referred to as domain D1 (Birnbaumer et al., 1998). The remaining sequence of both β_{4a} and β_{4b} is composed of 1410 nucleotides that encode the 470 amino acids of domains 2–5 (data not shown). As shown in Figure 1, exon 1 of β_{4a} encodes a 15 amino acid sequence that is highly homologous to the N-terminal sequences of several previously identified Ca^{2+} channel β_3 subunits. This indicates that β_{4a} exon 1 must have been present in the genome before the time that an ancestral gene duplicated to form distinct β_3 and β_4 genes. Interestingly, amino acids 5–11 (LYLHGIE) are identical to those found in the *Xenopus* β subunit, $x\beta_{32}$, but quite divergent from the same region of the human β_3 subunit. This could imply that a particular function of this sequence has been purposely conserved throughout evolution. Also of note in the human β_{4a} sequence are two D to N conversions at positions 4 and 12 (asterisks) that eliminate

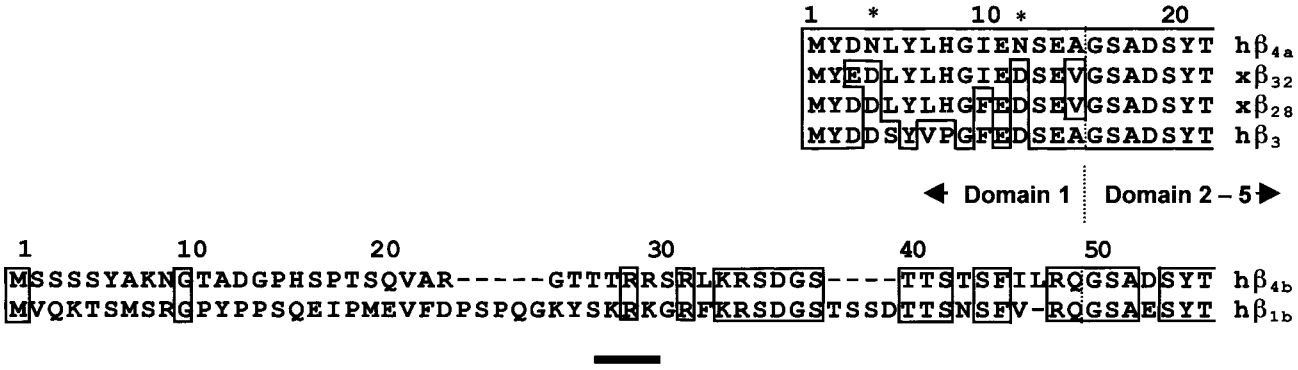

Figure 1. Sequence comparisons of human spinal cord Ca^{2+} channel β_{4a} and β_{4b} subunits and other β subunit subtypes. *Top*, The amino acid sequence of domain 1 and a short segment of domain 2 of the human β_{4a} subunit ($h\beta_{4a}$) is shown aligned with comparable domains of two *Xenopus* β_3 subunits ($x\beta_{32}$ and $x\beta_{28}$) (Tareilus et al., 1997) and a human β_3 subunit ($h\beta_3$). Amino acids identical to the $h\beta_{4a}$ sequence are *boxed. Asterisks* denote D to N amino acid conversions in the human β_{4a} sequence. *Bottom*, The amino acid sequence of domain 1 and a short segment of domain 2 of the human β_{4b} subunit ($h\beta_{4b}$) is shown aligned with comparable domains of the human β_{1b} subunit. Identical amino acids are *boxed. Dashed lines* indicate gaps in the sequence. The *bar* denotes consensus sites for phosphorylation by protein kinase C.

two negative charges that appear to be highly conserved among β_3 subunits. Figure 1 also demonstrates that D1 of β_{4a} is not at all homologous to D1 of β_{4b}. It can be seen, however, that D1 of β_{1b} and β_{4b} are more closely related than D1 of β_{4a} and β_{4b}. Domain 1 of β_{4b} contains 49 amino acids, 2 of which are negatively charged, and 8 of which are positively charged. Six of these positive charges are clustered in the center of the sequence close to consensus sites (TTR and TRR) for phosphorylation by protein kinase C. No further Prosite-listed consensus sites were found in the D1 sequences of either β_{4a} or β_{4b}.

Alternative splicing of the β_4 subunit N terminus affects Ca^{2+} channel expression

Critical to the interpretation of our expression data is the fact that some populations of *Xenopus* oocytes have been shown to express low levels of an endogenous β_3-like subunit that is capable of binding to and altering the gating properties of injected α_1 subunits (Tareilus et al., 1997). To test for this possibility in our oocytes, we conducted experiments in which we measured the time required for $\alpha_{1A}/\alpha_2\delta$, $\alpha_{1A}/\alpha_2\delta + \beta_{4a}$, and $\alpha_{1A}/\alpha_2\delta + \beta_{4b}$ complexes to reach levels of expression that we thought suitable for electrophysiological recording (1 μA of peak current). Figure 2 shows that channel complexes containing β_{4b} expressed at a much faster rate than those containing β_{4a}, reaching adequate levels within 1–2 d. Complexes containing β_{4a} took 3–4 d to reach similar levels, whereas complexes that did not contain a β subunit required 7–8 d to express 1 μA of current. Similarly, $\alpha_{1B}/\alpha_2\delta + \beta_{4b}$ complexes reached adequate levels in 1–2 d, whereas $\alpha_{1B}/\alpha_2\delta + \beta_{4a}$ complexes took 3–4 d to reach similar levels. α_{1B} complexes expressed without β_4 subunits did not reach suitable current size until day 7–8 (data not shown). $\alpha_{1C}/\alpha_2\delta$ and $\alpha_{1E}/\alpha_2\delta$ expressed with either β_{4a} or β_{4b} reached adequate current size in 6–8 d, whereas complexes without β_4 subunits showed no appreciable current even after 8 d. Expression rates and levels for $\alpha_{1C}/\alpha_2\delta$ and $\alpha_{1E}/\alpha_2\delta + \beta_{4a}$ and β_{4b} were essentially identical (data not shown). As shown in Figure 2, a sixfold increase in the amount of β subunit cRNA injected into oocytes relative to that of α_{1A} did not affect expression rates or levels, suggesting that β subunit binding sites on α_{1A} are saturated even when the two subunits are coinjected at a 1:1 ratio. This is consistent with the findings of Qin et al. (1996). We concluded from these experiments that the endogenous *Xenopus* β_3-like subunit would not significantly influence the examination of exogenous currents measured in the 2–6 d time period.

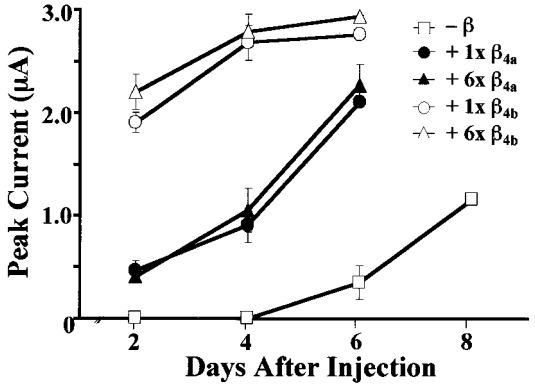

Figure 2. Expression rates of α_{1A} Ca^{2+} channel complexes with different β subunit compositions. Peak currents elicited by depolarization to +10 mV ($\alpha_{1A}/\alpha_2\delta$), +5 mV ($\alpha_{1A}/\alpha_2\delta + \beta_{4a}$), or 0 mV ($\alpha_{1A}/\alpha_2\delta + \beta_{4b}$) from a holding potential of −80 mV are plotted against days after injection. Barium (5 mM) was the charge carrier. Oocytes were maintained in ND96 culture media at 18°C. Comparisons between experiments in which the β_{4a} or β_{4b} subunits were injected at 1:1 (1×) or 6:1 (6×) ratios relative to the α_{1A} are shown. Each data point represents a minimum of six recordings. The SEM for each point is shown unless the values were smaller than the symbol.

Alternatively spliced β_4 subunits have α_1-subunit subtype-specific effects on voltage-dependent activation and inactivation

To determine whether β_4 N-terminal splicing affected Ca^{2+} channel gating properties, we expressed either β_{4a} or β_{4b} with rabbit $\alpha_2\delta$ and with rabbit α_{1A} (BI-2) (Mori et al., 1991), rat α_{1B} (Δ21 α_{1B}) (Pan and Lipscombe, 2000), rabbit α_{1C} (Mikami et al., 1989), or marine ray α_{1E} (doe-1) (Horne et al., 1993) in *Xenopus* oocytes. (The $\alpha_2\delta$-1 subunit is included in all experiments in this study.) Figure 3*A*,*B*,*E*,*F* shows comparisons of normalized current–voltage (*I–V*) curves for the four different α_1 subunits expressed with either β_{4a} or β_{4b}. Figure 3, *A* and *B*, illustrate that the peaks of the current–voltage curves for α_{1A} and α_{1B} complexes containing β_{4b} were shifted to more hyperpolarized potentials relative to complexes containing β_{4a}. In contrast, Figure 3, *E*

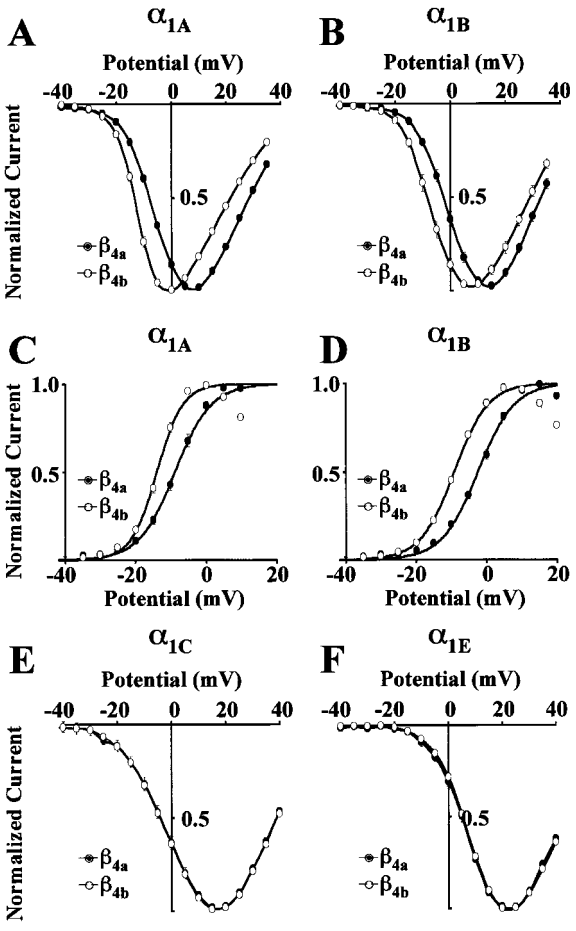

Figure 3. β_{4a} and β_{4b} subunits have α_1 subunit subtype-specific effects on the voltage dependence of activation. *A*, *B*, *E*, *F*, Normalized, averaged peak current–voltage (*I–V*) plots for α_{1A} (*A*), α_{1B} (*B*) α_{1C} (*E*), and α_{1E} (*F*) coexpressed with $\alpha_2\delta$ and either β_{4a} or β_{4b}. *A*, *B*, The α_{1A} (BI-2) and α_{1B} (Δ21) subunits used in these and subsequent experiments are those described by Mori et al. (1991) and Pan and Lipscombe (2000), respectively. Currents were activated by 300 msec depolarizations to various test potentials (−40 to +40 mV in 5 mV increments) from a holding potential of −80 mV. Barium (5 mM) was the charge carrier for both α_{1A} and α_{1B}. *C*, *D*, Voltage dependence of activation up to +10 mV for α_{1A} (*C*) and +20 mV for α_{1B} (*D*) as determined from averaged *I–V* data in *A* and *B*. Data points represent the means of the normalized data at a given membrane potential. The SEM for each point is shown unless the values were smaller than the symbol. *Smooth curves* represent a single Boltzmann fit to the averaged data. Values for $V_{1/2}$ and *k* for α_{1A} and α_{1B} plus α_2/δ and either β_{4a} or β_{4b} are listed in Table 1. *E*, *F*, The α_{1C} (cardiac) and α_{1E} (doe-1) subunits used in these and subsequent experiments are those described by Mikami et al. (1989) and Horne et al. (1993), respectively. Currents were activated by 300 msec depolarizations to various test potentials (−40 to +40 mV in 5 mV increments) from a holding potential of −80 mV ($\alpha_{1C} + \beta_{4a}$, $n = 12$; $\alpha_{1C} + \beta_{4b}$, $n = 13$; $\alpha_{1E} + \beta_{4a}$, $n = 9$; $\alpha_{1E} + \beta_{4b}$, $n = 9$). Barium (40 mM) was the charge carrier.

and *F*, shows that the *I–V* curves for α_{1C} and α_{1E} complexes containing either β_{4a} or β_{4b} were essentially superimposed. The difference in α_1 subunit responsiveness was not caused by differences in charge carrier concentrations used in the experiments (5 mM Ba^{2+} for α_{1A} and α_{1B}; 40 mM Ba^{2+} for α_{1C} and α_{1E}), because we observed identical hyperpolarizing shifts for both α_{1A} and α_{1B} with β_{4b}, even in 40 mM Ba^{2+} (data not shown). We concluded from these first experiments that alternative splicing of the β_4 subunit N terminus affects activation of Ca^{2+} channel complexes containing α_{1A} and α_{1B} subunits but not those containing α_{1C} or α_{1E}. To estimate the $V_{1/2}$ of activation for the different α_{1A} and α_{1B} combinations, we averaged Boltzmann fits to the *I–V* data generated over the range of −40 to +10 mV for α_{1A} complexes and −40 to +20 mV for α_{1B} complexes containing either β_{4a} or β_{4b} (Fig. 3*C*,*D*). The results show that the $V_{1/2}$ of activation for both α_{1A} and α_{1B} complexes containing β_{4b} were shifted to the left relative to complexes containing β_{4a} by ~5 mV and ~7 mV, respectively (Table 1). The results also show that the slopes of the β_{4b} fits were somewhat steeper than for β_{4a}.

We next examined whether alternative splicing of the β_4 subunit affected isochronal inactivation. We used a 20 sec conditioning prepulse over a wide range of potentials followed by a 300 msec test pulse to near-peak potentials to generate the data. Figure 4*A–D* shows that, as was the case for activation, alternative splicing of the β_4 subunit N terminus affects inactivation of Ca^{2+} channel complexes containing α_{1A} and α_{1B} subunits but not those containing α_{1C} or α_{1E}. The figure illustrates that the voltage dependence of inactivation of both α_{1A} (Fig. 4*A*) and α_{1B} (Fig. 4*B*) complexes containing β_{4b} was shifted to more hyperpolarized potentials relative to complexes containing β_{4a}. In contrast, inactivation curves for α_{1C} (Fig. 4*C*) and α_{1E} (Fig. 4D) complexes containing β_{4a} or β_{4b} were essentially identical. The Boltzmann-derived $V_{1/2}$ for inactivation of both α_{1A} and α_{1B} complexes containing β_{4b} were shifted to the left relative to complexes containing β_{4a} by ~10–11 mV (Table 1). Interestingly, the hyperpolarizing shift in $V_{1/2}$ for α_{1A} complexes (Fig. 4*A*) occurred as the result of a parallel shift in the voltage dependence of inactivation, whereas for α_{1B} complexes (Fig. 4*B*), the shift in $V_{1/2}$ occurred primarily as the result of a change in slope. Slope factors for α_{1B} complexes containing β_{4a} and β_{4b} complexes were ~14 and 7 mV, respectively (Table 1).

Because α_{1C} and α_{1E} subunits were not affected by alternative splicing of β_4 subunits, we next directed our experiments toward characterizing the α_{1A} and α_{1B} responses in more detail. Figure 5 shows representative current traces of α_{1A} (Fig. 5*A*) and α_{1B} (Fig. 5*B*) complexes containing either β_{4a} (*top*) or β_{4b} (*bottom*) expressed in *Xenopus* oocytes. Traces shown were generated by step depolarization to −10, 0, 10, 20, and 30 mV. The *arrows* indicate that the potentials at which peak currents were reached varied with each complex. Regardless of the α_1 subunit subtype, however, complexes containing β_{4a} inactivated faster than those containing $\beta_{4b,}$ with a difference in rates being more apparent for complexes containing α_{1B}. Figure 5, *C* and *D*, shows the averaged currents remaining after 300 msec (R_{300}) step depolarizations to each potential for α_{1A} and α_{1B}, respectively. The results indicate that the rate of inactivation for all four complexes is voltage dependent and that the differences in rates between complexes containing β_{4a} versus β_{4b} become apparent primarily with depolarizations beyond 0 mV.

α_1 subunit-specific responses to β_4 subunit N- and C- terminal deletions

The results to this point indicated that the N terminus of the β_4 subunit plays an important role in setting the kinetics and voltage-dependence of Ca^{2+} channel gating, with some differences in responsiveness noted between α_{1A} and α_{1B} subunits. We next sought to determine whether the β_4 N terminus could be acting in concert with the β_4 C terminus to exert its effects on gating. Because previous studies had shown that the β_4 C terminus binds directly to the α_{1A} subunit (Walker et al., 1998, 1999), it was of particular interest to determine whether the gating properties of α_{1A} would change in comparison to α_{1B} if the β_4 C terminus were

Table 1. Effects of β_4 subunit alternative splicing and N- and C-terminal deletions on voltage-dependent activation and inactivation of α_{1A} and α_{1B} Ca^{2+} channel subunits

	α_{1A}					α_{1B}				
	β	$V_{1/2}$ (*mV*)	*k* (*mV*)	*z*	*n*	β	$V_{1/2}$ (*mV*)	*k* (*mV*)	*z*	*n*
Boltzmann-derived values for activation										
A_1	β_{4b}	−14.1 ± 0.4	3.5 ± 0.1	7.1	15	β_{4b}	−9.9 ± 0.6	4.2 ± 0.1	5.9	15
	$\beta_{4a}\Delta C$	−12.0 ± 0.5	3.6 ± 0.2	6.9	13	$\beta_4\Delta N$	−9.3 ± 1.2	4.8 ± 0.3	5.2	11
	$\beta_4\Delta N\Delta C$	−15.3 ± 0.6	3.7 ± 0.5	6.8	11	$\beta_4\Delta N\Delta C$	−8.0 ± 0.5	4.6 ± 0.2	5.4	14
A_2	β_{4a}	−8.4 ± 0.6	4.8 ± 0.1	5.2	12	β_{4a}	−2.3 ± 0.6	5.0 ± 0.1	5.0	16
	$\beta_{4b}\Delta C$	−8.8 ± 0.4	4.1 ± 0.2	6.0	16	$\beta_{4a}\Delta C$	−3.3 ± 0.5	4.2 ± 0.2	6.0	11
	$\beta_4\Delta N$	−8.9 ± 0.5	4.6 ± 0.1	5.4	14	$\beta_{4b}\Delta C$	−2.6 ± 1.0	4.0 ± 0.4	6.2	11
Boltzmann-derived values for inactivation										
I_1	$\beta_{4a}\Delta C$	−34.0 ± 0.8	8.0 ± 0.3	3.1	13	β_{4b}	−40.0 ± 2.6	13.0 ± 1.1	1.9	9
	$\beta_{4b}\Delta C$	−34.7 ± 0.9	8.2 ± 0.3	3.0	14	$\beta_4\Delta N$	−44.1 ± 1.3	14.2 ± 0.6	1.8	9
	$\beta_4\Delta N\Delta C$	−35.9 ± 0.9	7.9 ± 0.3	3.2	12	$\beta_4\Delta N\Delta C$	−41.6 ± 1.6	12.9 ± 0.8	1.9	10
I_2	β_{4a}	−29.7 ± 0.7	5.9 ± 0.3	4.3	10	β_{4a}	−31.4 ± 0.6	8.0 ± 0.9	3.1	8
	$\beta_4\Delta N$	−31.1 ± 0.7	6.3 ± 0.4	4.0	8	$\beta_{4a}\Delta C$	−32.1 ± 0.9	7.5 ± 0.3	3.3	10
					9	$\beta_{4b}\Delta C$	−31.9 ± 1.1	7.3 ± 0.4	3.4	8
I_3	β_{4b}	−40.3 ± 0.8	6.6 ± 0.4	3.8						

Values for activation and inactivation parameters ($V_{1/2}$ = midpoint; *k* = slope factor) derived from averaged Boltzmann fits to the data. Charge, *z*, was calculated by dividing 25 (approximate value for *RT*/*F* at room temperature, where *R* = gas constant, *T* = temperature, and *F* = Faraday constant) by the slope factor. Similar values are grouped into distinct modes, A_1, A_2, and I_1–I_3.

deleted. To address this issue, we made four β_4 subunit deletion constructs that along with β_{4a} and β_{4b} provided us with all the possible +/− combinations of β_4 N- and C termini (Fig. 6*A*). We found that all four constructs augmented Ca^{2+} channel expression to a level that was comparable to or exceeded (i.e., $\beta_4\Delta N\Delta C$) the expression levels we observed with β_{4b}. The effects of these constructs on activation and inactivation of α_{1A} and α_{1B} subunits are shown in Figure 6, *B* and *C*, and Figure 7, *A* and *B*, respectively. (Our initial results with β_{4a} and β_{4b} are included as *dashed lines* for reference in Figs. 6 and 7). Interestingly, it was readily apparent from both the activation and inactivation results shown in Figures 6 and 7 that despite testing six different β_4 subunit constructs, our data could be grouped into two activation modes, A_1 and A_2 (α_{1A} and α_{1B}), and two (α_{1B}) or three (α_{1A}) inactivation modes, I_1–I_3, on the basis of the curve position alone. As can be seen from the data, the distinction between activation and inactivation modes was most clearly delineated in experiments involving α_{1B} (Figs. 6*C*, 7*B*). Table 1 shows that the distinction between modes is quite evident when comparing Boltzmann-derived values for $V_{1/2}$ and slope factor, and along with Figures 6 and 7 reveals that the β_4 subunit constructs responsible for setting each mode differ between α_{1A} and α_{1B} subunits.

The details of the deletion results are best understood by examining in sequence the data that we obtained with individual β subunit constructs. Our first experiments were directed toward determining what effect deletion of both the β_4 N and C termini ($\beta_4\Delta N\Delta C$) would have on α_{1A} and α_{1B} gating properties. Unexpectedly, both α_{1A} and α_{1B} complexes containing the $\beta_4\Delta N\Delta C$ subunit had activation properties very similar to complexes containing full-length β_{4b} (Fig. 6*B*,*C*, mode A_1). This indicated that α_1 subunits could not distinguish β_4 subunits without an N or C terminus from β_4 subunits with the longer form of N terminus and the C terminus present. Relative to α_1 complexes containing β_{4a}, however, $\beta_4\Delta N\Delta C$ caused a 6–7 mV hyperpolarizing shift and a slight increase in slope of activation of both α_{1A} and α_{1B} (Table 1). Figure 7, *A* and *B*, shows that, although the inactivation curve for α_{1A} complexes containing $\beta_4\Delta N\Delta C$ fell between those for

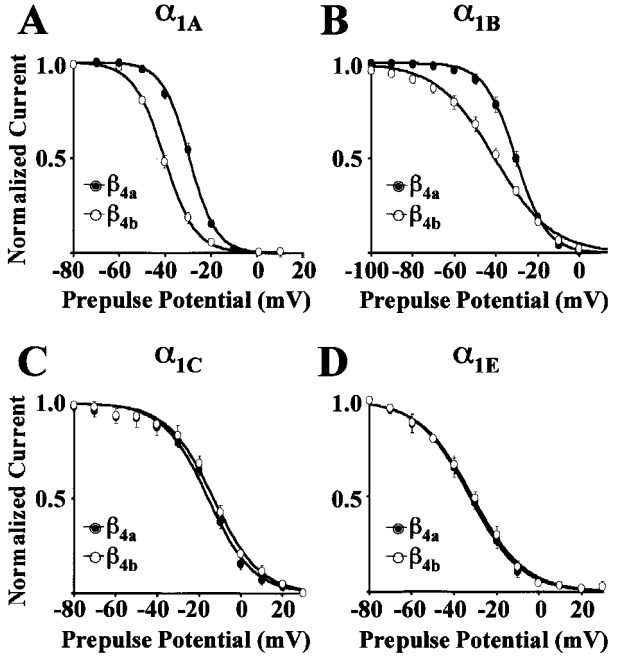

Figure 4. β_{4a} and β_{4b} subunits have α_1 subunit subtype-specific effects on the voltage dependence of inactivation. *A–D*, Normalized, averaged isochronal inactivation curves for α_{1A} (*A*), α_{1B} (*B*), α_{1C} (*C*), and α_{1E} (*D*) coexpressed with $\alpha_2\delta$ and either β_{4a} or β_{4b}. Curves were generated from peak currents elicited by a 300 msec test depolarization to +5 mV (α_{1A} + β_{4a}), 0 mV (α_{1A} + β_{4b}), +10 mV (α_{1B} + β_{4a}), +5 mV (α_{1B} + β_{4b}), or +20 mV (α_{1C} and α_{1E} with β_{4a} and β_{4b}) after a 20 sec conditioning prepulse to voltages ranging from −80 to +30 mV (*A*, *C*, *D*) or −100 to +10 mV (*B*). Barium (5 mM for α_{1A} and α_{1B}; 40 mM for α_{1C} and α_{1E}) was the charge carrier. Data points represent the means of the normalized data at a given membrane potential. The SEM for each point is shown unless the values were smaller than the symbol. *Smooth curves* represent a single Boltzmann fit to the averaged data. Values for $V_{1/2}$ and *k* for inactivation of α_{1A} and α_{1B} plus $\alpha_2\delta$ and either β_{4a} or β_{4b} are listed in Table 1.

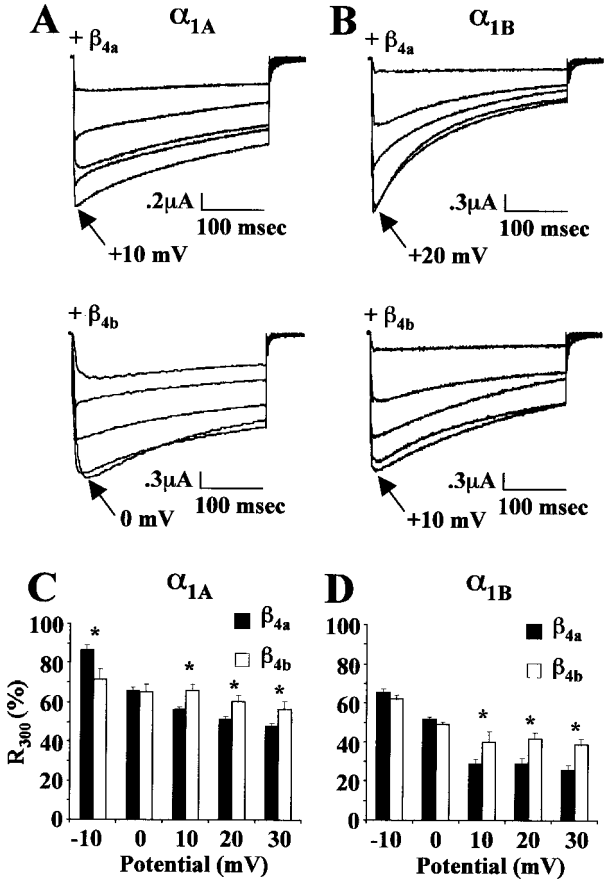

Figure 5. α_{1A} and α_{1B} complexes containing β_{4a} inactivate faster than those containing β_{4b}. *A*, *B*, Representative current traces of α_{1A} (*A*) and α_{1B} (*B*) plus $\alpha_2\delta$ and either β_{4a} (*top*) or β_{4b} (*bottom*). Currents were elicited by step depolarizations to a range of test potentials (−10 to +30 mV in 10 mV increments) from a holding potential of −80 mV. Barium (5 mM) was used as the charge carrier. Traces were fit with a single exponential from 25 msec beyond the peak inward current to the end of the depolarization. Averages of $\tau_{inactivation}$ at the peak current potential were $\alpha_{1A} + \beta_{4a}$, 226.6 ± 12.5 msec ($n = 12$); $\alpha_{1A} + \beta_{4b}$, 307.2 ± 19.2 msec ($n = 10$); $\alpha_{1B} + \beta_{4a}$, 160.1 ± 20.0 msec ($n = 10$); $\alpha_{1A} + \beta_{4b}$, 213.9 ± 15.6 msec ($n = 10$). *C*, *D*, Current remaining at the end of a 300 msec test pulse (R_{300}), elicited as in the protocol above, for α_{1A} (*C*) and α_{1B} (*D*) plus $\alpha_2\delta$ and either β_{4a} or β_{4b}. The SEM for each bar is shown. *Asterisks* denote statistical significance ($p < 0.05$) as determined by a Student's two-sample equal variance *t* test.

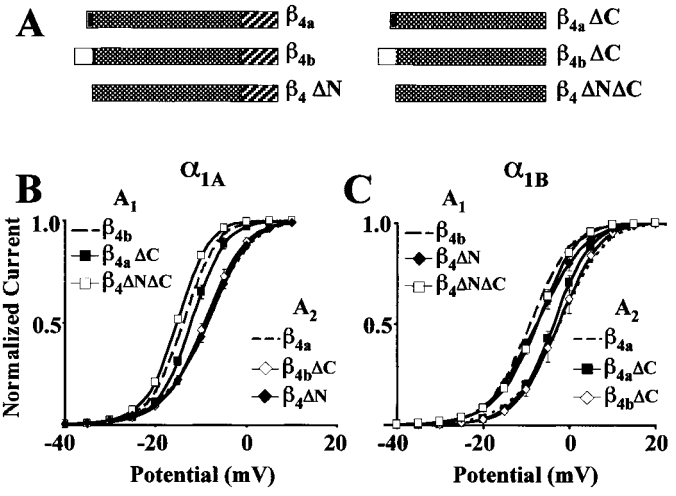

Figure 6. Effects of β_4 subunit N- and C-terminal deletions on the voltage dependence of activation of α_{1A} and α_{1B} Ca^{2+} channels. *A*, Schematic diagrams of the wild-type and artificial β_4 subunits used in this series of experiments. The 15 amino acid β_{4a} and 49 amino acid β_{4b} N termini (alternatively spliced forms of domain 1) are denoted by *filled* and *open bars*, respectively. Domains 2–4 are represented by a single *cross-hatched bar*. The C terminus (domain 5) is denoted by a *diagonally striped bar*. *B*, *C*, Voltage dependence of activation up to +10 mV for α_{1A} (*B*) and +20 mV for α_{1B} (*C*) as determined from averaged *I–V* data. Data points represent the means of the normalized data at a given membrane potential. The SEM for each point is shown unless the values were smaller than the symbol. *Smooth curves* represent a single Boltzmann fit to the averaged data. *Broken curves* represent activation data shown in Figure 3, *C* and *D*, and are included in this figure for reference. Values for $V_{1/2}$ and *k* for α_{1A} and α_{1B} plus α_2/δ and each of the six β_4 constructs are grouped according to curve similarities in Table 1.

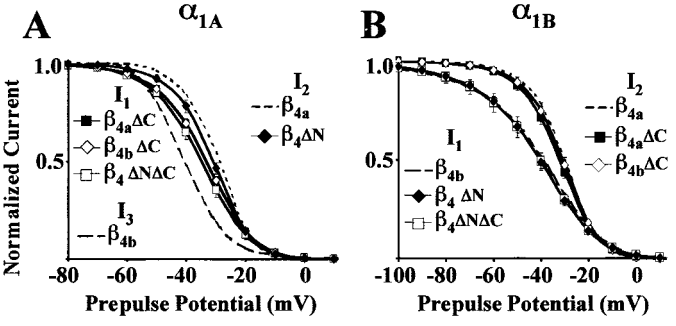

Figure 7. Effects of β_4 subunit N- and C-terminal deletions on the voltage dependence of inactivation of α_{1A} and α_{1B} Ca^{2+} channels. *A*, *B*, Normalized, averaged steady-state inactivation curves for α_{1A} (*A*) and α_{1B} (*B*) coexpressed with $\alpha_2\delta$ and one of the six β_4 constructs shown in Figure 6*A*. Curves were generated from peak currents elicited by a 300 msec test depolarization to −5 mV ($\alpha_{1A} + \beta_4\Delta N\Delta C$), 0 mV ($\alpha_{1A} + \beta_{4b}$, $\beta_{4a}\Delta C$), +5 mV ($\alpha_{1A} + \beta_{4a}$, $\beta_4\Delta N$, and $\beta_{4b}\Delta C$; $\alpha_{1B} + \beta_{4b}$ and $\beta_4\Delta N$), +10 mV ($\alpha_{1B} + \beta_{4a}$, $\beta_4\Delta N\Delta C$), or +15 mV ($\alpha_{1B} + \beta_{4a}\Delta C$ and $\beta_{4b}\Delta C$) after a 20 sec conditioning prepulse to voltages ranging from −80 to +10 mV (*A*) or −100 to +10 mV (*B*). Barium (5 mM) was the charge carrier for both α_{1A} and α_{1B}. Data points represent the means of the normalized data at a given membrane potential. The SEM for each point is shown unless the values were smaller than the symbol. *Smooth curves* represent a single Boltzmann fit to the averaged data. Values for $V_{1/2}$ and *k* for inactivation of α_{1A} and α_{1B} plus $\alpha_2\delta$ and each of the six β_4 constructs are grouped according to curve similarities in Table 1.

complexes containing β_{4a} and β_{4b}, the inactivation properties of α_{1B} complexes containing $\beta_4\Delta N\Delta C$ and β_{4b} were also indistinguishable. For both α_{1A} and α_{1B}, it can be seen that relative to complexes containing β_{4a}, $\beta_4\Delta N\Delta C$ caused a qualitatively similar hyperpolarizing shift in the voltage dependence of inactivation and decrease in slope (shift from mode I_2 to mode I_1). As shown in Figure 7*B*, this effect was most dramatic for α_{1B} complexes, where relative to β_{4a}, $\beta_4\Delta N\Delta C$ caused a ~10 mV hyperpolarizing shift in inactivation and a nearly 50% decrease in slope (Table 1).

We next characterized the effects of the construct $\beta_4\Delta N$ ($\beta_4\Delta N\Delta C$ plus the β_4 C terminus) on the gating properties of α_{1A} and α_{1B} subunits. Interestingly, as shown in Figure 6, *A* and *B*, the $\beta_4\Delta N$ construct had different effects on activation of α_{1A} as compared with α_{1B}. Although addition of the C terminus had a depolarizing effect on α_{1A} activation relative to β_{4b} and $\beta_4\Delta N\Delta C$, there was no change in the activation properties of α_{1B}. Moreover, as can be seen in Figure 6*B* and Table 1, the activation properties of α_{1A} complexes containing $\beta_4\Delta N$ were essentially identical to those containing β_{4a} (mode A_2). Similarly, as shown in Figure 7, *A* and *B*, $\beta_4\Delta N$, like β_{4a}, had a noticeable depolarizing effect on α_{1A} inactivation (mode I_2) relative to complexes

containing $\beta_4\Delta N\Delta C$ but caused no change in the inactivation properties of α_{1B}. These results indicated that, at least in the absence of the N terminus, the β_4 C terminus has α_{1A} subunit-specific effects on the voltage dependence of both activation and inactivation.

To define further the role of the β_4 N termini in gating, we next characterized the effects of two constructs, $\beta_{4a}\Delta C$ and $\beta_{4b}\Delta C$, that lacked the β_4 C terminus but contained the N termini of β_{4a} and β_{4b}, respectively ($\beta_4\Delta N\Delta C$ plus β_{4a} or β_{4b} N terminus). Interestingly, the pattern of results that we obtained with these constructs in many respects was just the opposite of what we saw with $\beta_4\Delta N$. Although $\beta_4\Delta N$ had α_{1A} subunit-specific effects on gating, $\beta_{4a}\Delta C$ and $\beta_{4b}\Delta C$ had, for the most part, α_{1B} subunit-specific effects. Figure 6*A* shows that relative to $\beta_4\Delta N\Delta C$, $\beta_{4b}\Delta C$, like β_{4a}, caused a depolarizing shift in activation of α_{1A} subunits, but $\beta_{4a}\Delta C$ was without effect. Figure 7*A* shows that relative to $\beta_4\Delta N\Delta C$, neither $\beta_{4a}\Delta C$ nor $\beta_{4b}\Delta C$ had effects on inactivation of α_{1A} subunits. In contrast, Figures 6*B* and 7*B* show that relative to $\beta_4\Delta N\Delta C$ both $\beta_{4a}\Delta C$ and $\beta_{4b}\Delta C$ caused a depolarizing shift in activation and inactivation of α_{1B}. Moreover, the gating properties of α_{1B} complexes containing $\beta_{4a}\Delta C$ or $\beta_{4b}\Delta C$ were essentially identical to those containing β_{4a} (modes A_2 and I_2). The results of these experiments indicate that, at least in the absence of the C terminus, the β_{4b} but not the β_{4a} N terminus has effects on α_{1A} activation, whereas neither affects α_{1A} inactivation. In contrast, both the β_{4a} and β_{4b} N termini have effects on α_{1B} activation and inactivation.

With the results from the deletion experiments, it was informative to reexamine the data from our initial experiments (Figs. 6 and 7, *dashed lines*) with the idea that full-length β_{4a} and β_{4b} subunits were constructed by adding back the β_{4a} and β_{4b} N termini to $\beta_4\Delta N$. As the data reveals, this also had α_1 subunit-specific effects on both activation and inactivation. With respect to activation, Figure 6*A* shows that, relative to $\beta_4\Delta N$, adding back the β_{4a} N terminus had no effect on α_{1A} activation, suggesting that the short form of N terminus could not overcome the α_{1A}-specific β_4 C-terminal effect noted with $\beta_4\Delta N$ previously. Adding back the β_{4b} N terminus, however, did supercede the C-terminal effect and caused a hyperpolarizing shift in α_{1A} activation relative to $\beta_4\Delta N$ (back to mode A_1). In contrast, Figure 6*B* shows that adding back the β_{4a} N terminus to $\beta_4\Delta N$ caused a depolarizing shift in the activation of α_{1B} (back to mode A_2), but adding back the β_{4b} N terminus had no effect. This goes along with the $\beta_4\Delta N$ data showing that with α_{1B} there is no β_4 C-terminal effect to overcome, and that the β_{4a} N terminus alone causes an α_{1B}-specific depolarizing shift in activation. With respect to inactivation, Figure 7*B* shows that, as was the case for activation, adding back the β_{4a} N terminus to $\beta_4\Delta N$ had little effect on α_{1A} inactivation, but adding back the β_{4b} N terminus caused a significant hyperpolarizing and, in this case, parallel shift in the curve for α_{1A} inactivation (mode I_3). It is worth noting that this shift is different from and goes beyond the curve for $\beta_4\Delta N\Delta C$, and that this effect on α_{1A} gating is unique to β_{4b}. Figure 7*B* shows that, as expected from the $\beta_{4a}\Delta C$ results with α_{1B}, without a C-terminal effect to overcome, adding back the β_{4a} N terminus to $\beta_4\Delta N$ caused a depolarizing shift in α_{1B} inactivation (back to mode I_2). Not expected, however, was the result that adding back the β_{4b} N terminus had no effect, recalling that the β_{4b} N terminus alone causes a depolarizing shift in α_{1B} inactivation. This suggests that the presence of the β_4 C terminus, although not having effects on its own, interferes in some way with the ability of the β_{4b} N terminus to influence α_{1B} channel gating.

DISCUSSION

Our results provide the first evidence that alternative splicing of the β_4 subunit alters Ca^{2+} channel gating and that this effect is specific to α_{1A} and α_{1B} subunits. The physiological relevance of our findings lies in the fact that α_{1A}, α_{1B} (Westenbroek et al., 1998), and β_4 subunits (Wittemann et al., 2000) colocalize in nerve terminals and that α_{1A} and β_4 (Liu et al., 1996) and α_{1B} and β_4 subunits (Scott et al., 1996) are directly associated. In many respects, our experiments were similar to those of Olcese et al. (1994) and Qin et al. (1996), which characterized the effects of various β subunit splice variants, chimeras, and deletion mutants on human α_{1E} subunit gating. Their studies yielded five results pertinent to our findings. (1) Relative to α_{1E} alone, all β subunit constructs tested caused a nearly identical hyperpolarizing shift in the $V_{1/2}$ of activation and decrease in slope factor [see also Jones et al. (1998)]. (2) Deletion of the N terminus of the β_{1b}, β_{2a}, and β_3 subunits had no effect on the fast component of activation. (3) Alternative splicing of the N terminus, C terminus, and internal domain 3 of β_1 and β_2 subunits had opposing effects on the $V_{1/2}$ of steady-state inactivation but did not affect slope. (4) Deletion of the N terminus of the β_{1b} and β_3 subunits caused a depolarizing shift in the $V_{1/2}$ of inactivation without affecting slope, whereas deletion of the N terminus of the β_{2a} subunit caused a hyperpolarizing shift. (5) C-terminal alternative splicing did not affect gating properties. The principal conclusion of these experiments was that, independent of effects on activation, the N terminus of the β subunit plays a dominant role in governing the voltage sensitivity of α_{1E} subunit inactivation. This suggested to Olcese et al. (1994) that there were two separate α_1 and β subunit interaction sites regulating activation and inactivation.

Our results point similarly to the N terminus of the β_4 subunit as a key determinant of α_{1A} and α_{1B} gating properties but show some dissimilarity to the five α_{1E} results listed above. (1) Unlike α_{1E} with β_1–β_3 subunits, alternatively spliced β_4 subunits had differential effects on activation of both α_{1A} and α_{1B}. Relative to the short β_{4a} N terminus, the longer β_{4b} form caused a hyperpolarizing shift in activation of both α_{1A} and α_{1B} subunits (but not α_{1C} or α_{1E}). (2) Relative to β_{4b}, deletion of the N terminus of the β_4 subunit caused a depolarizing shift in activation of α_{1A} but not α_{1B}. (3) Alternative splicing of the β_4 subunit affected both the $V_{1/2}$ and slope of inactivation of α_{1B}, whereas only shifting the $V_{1/2}$ of α_{1A} inactivation without a change in slope. Alternative splicing of the β_4 subunit did not affect inactivation of α_{1C} or α_{1E}. (4) Relative to β_{4b}, deletion of the N terminus of the β_4 subunit caused a depolarizing shift in inactivation of α_{1A} but not α_{1B}. (5) C-terminal deletion experiments revealed that the β_4 N and C termini work in concert to set gating parameters of α_{1A} and α_{1B} subunits. Taken together, these results indicate that alternatively spliced β subunits can affect both activation and inactivation of Ca^{2+} channels, and the responsiveness of Ca^{2+} channels to β subunit splicing varies with α_1 subunit subtype.

To explain our results, we devised a structural model for potential α_1–β_4 subunit domain interactions based on a β subunit modular structure (domains A–E) (Hanlon et al., 1999) and actual molecular weights of the potential α_{1A} and β subunit domains involved (Fig. 8). Although highly speculative, the model integrates related structure–function results from a number of different laboratories that point to the β subunit D domain interaction with the α_1 subunit I–II linker as a key determinant of Ca^{2+} channel gating properties (Herlitze et al., 1997; Bourinet et al., 1999; Stotz et al., 2000; Berrou et al., 2001). Moreover, it

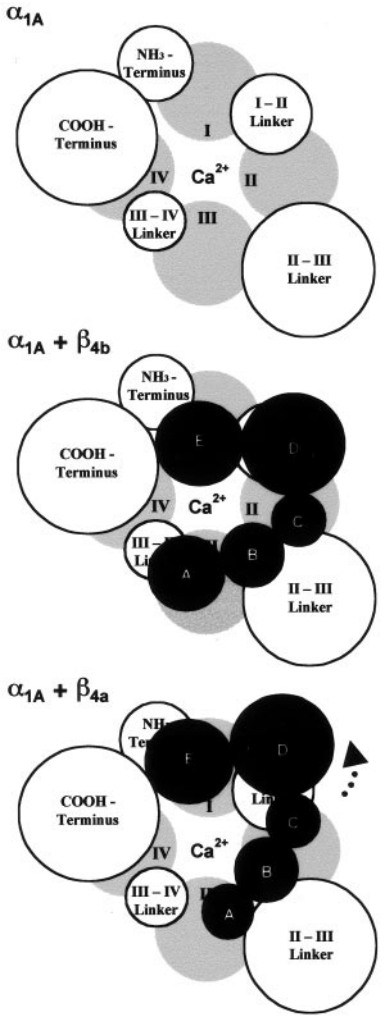

Figure 8. Potential α_{1A} and β subunit domain interactions as viewed from inside the cell looking out through the pore. *Top*, α_{1A} alone. Transmembrane domains *I–IV* are represented as *gray circles* and intracellular domains as *white circles. Middle*, $\alpha_{1A} + \beta_{4b}$. The β_{4b} subunit *A–E* domains are shown as *black circles* superimposed on α_{1A}. *Bottom*, $\alpha_{1A} + \beta_{4a}$. The radius of each *circle* was calculated from the spherical volume ($V = 4/3\ \pi r^3$) of each subunit domain, where $V = [(0.73\ cm^3/gm \times 10^{24}\ Å^3/cm^3 \times \text{molecular weight})/6.02 \times 10^{23}]$ and the average molecular weight of an amino acid is 120 Da. For α_{1A} (BI-2): N terminus, 98 aa; transmembrane domains I–IV, 229–268 aa; I–II linker, 127 aa; II–III linker, 537 aa; III–IV linker, 54 aa; C terminus, 604 aa. For β_{4b} [nomenclature as in Hanlon et al. (1999)]: A domain, 92 aa; B domain, 61 aa; C domain, 37 aa; D domain, 210 aa; E domain, 144 aa. For β_{4a}: A domain, 44 aa. Interactions of the β_4 D domain with the α_{1A} I–II linker (Pragnell et al., 1994) and β_4 E domain with α_{1A} N and C termini have been well documented (Walker et al., 1998, 1999). *Dashed arrow* in the *bottom diagram* indicates the potential for a conformational change when the β_{4a} N terminus is substituted for the β_{4b} N terminus.

incorporates results showing that regulation of activation and inactivation are separable functions of β subunits (Olcese et al., 1994). Of particular relevance to our model are studies showing that the β_1 subunit D domain was all that was required to reproduce the inactivation rate of L-type channels coexpressed with full-length β_1 (Cens et al., 1999) and that a single point mutation (R378E) in the β subunit binding site of the α_1 I–II linker (AID domain) had a depolarizing effect on the voltage dependence of both activation and inactivation of an α_{1E} subunit (Berrou et al., 2001).

Table 2. Gating mode model describing the effects of β_4 subunit constructs on α_{1A} and α_{1B} subunit activation and inactivation

	β Subunit	Mode	Activation	Inactivation
1	ΔN ΔC (α_{1A})	$A_1 I_1$	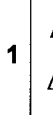	
	ΔN ΔC (α_{1B})	$A_1 I_1$		
2	ΔN (α_{1A})	$A_2 I_2$		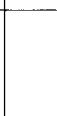
	ΔN (α_{1B})	$A_1 I_1$		
3	β_{4a} ΔC (α_{1A})	$A_1 I_1$	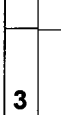	
	β_{4a} ΔC (α_{1B})	$A_2 I_2$		
4	β_{4b} ΔC (α_{1A})	$A_2 I_1$		
	β_{4b} ΔC (α_{1B})	$A_2 I_2$		
5	β_{4a} (α_{1A})	$A_2 I_2$	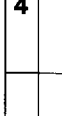	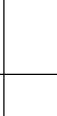
	β_{4a} (α_{1B})	$A_2 I_2$		
6	β_{4b} (α_{1A})	$A_1 I_3$	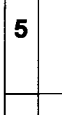	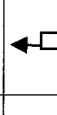
	β_{4b} (α_{1B})	$A_1 I_1$		

Gating modes induced by each β subunit described in terms of separate α_1–β interaction points for activation and inactivation (α_1, filled symbols; β, open symbols). Arrows indicate potential displacement of the β subunit in either N- or C-terminal direction.

Previous studies have shown that the D domain of the β_4 subunit binds with high affinity to the α_{1A} I–II linker (Pragnell et al., 1994) and that the E domain of the β_4 subunit binds to both the N and C terminus of the α_{1A} subunit (Walker et al., 1998, 1999). As shown in Figure 8, this indicates that the D and E domains likely establish the N- to C-terminal orientation of the β_4 subunit relative to the α_{1A} subunit. Although little is known about β subunit N-terminus interactions with the α_1 subunit, a modular structure for the β subunit A, B, and C domains suggests that the interactions could occur over a wide range. As suggested in Figure 8, a change in the size and sequence of the β subunit A domain could have an effect on the way the β subunit D domain interacts with the α_1 I–II linker. Such a change might be responsible for the different gating properties observed between Ca^{2+} channel complexes containing β_{4a} versus β_{4b}.

The salient feature of the model is that a core β subunit structure encoded by exons 2–12 (β_4ΔNΔC), through interactions with the α_1 subunit I–II linker, sets separate default parameters for α_1 activation and inactivation (Table 2, mode A_1I_1). This mode likely represents a specific α_1 I–II linker conformation that, through its connection to the α_1 IS6 transmembrane domain, influences the mobility of the gating charges within α_1 IS4 (Zhang et al., 1994). [The effects of β_4 N-terminal alternative splicing on apparent gating charge (z value) are shown in Table 1. Note the

significant difference in calculated z values during inactivation of α_{1B} complexes containing β_{4a} versus β_{4b}.] As shown in Table 2, in mode A_1I_1 the two presumed α_1 and β subunit interaction domains are in alignment (α_1, filled symbols; β, open symbols). Changes from default parameters occur when either the β subunit N or C terminus, or both, interacts with, or is acted on by, other regions of the α_1 subunit such that the I–II linker changes mode conformations. For example, in mode A_2I_2 (row 2), the two presumed α_1 and β subunit interaction domains would be out of alignment. Displacing the β subunit D domain in either the C- or N-terminal direction would enable mode 2 conformation, whereas a balance of these two forces favors mode 1.

Describing our data in terms of the model (Table 2), the default activation and inactivation parameters of α_{1A} and α_{1B} complexes containing $\beta_4\Delta N\Delta C$ are denoted as mode A_1I_1 (row 1). Steep activation and shallow inactivation typify this mode. Row 2 shows that adding back the C terminus to $\beta_4\Delta N\Delta C$ ($\beta_4\Delta N$) shifts α_{1A} complexes to mode A_2I_2, whereas α_{1B} complexes remain in mode A_1I_1. This could be explained by the α_{1A}–β_4 C-terminal binding event described by Walker et al. (1998, 1999) causing the β_4 D domain to be displaced in the C-terminal direction. Relative to mode A_1I_1, activation in mode A_2I_2 is shallower and inactivation is steeper. Rows 3 and 4 show that by adding back the N terminus, α_{1B} complexes containing either the $\beta_{4a}\Delta C$ or $\beta_{4b}\Delta C$ construct shift to mode A_2I_2. This shift might be explained by β_4 N-terminal-α_{1B} interactions causing the β_4 D domain to be displaced in the N-terminal direction. Alternatively, steric changes resulting from the presence of the N terminus may shift the β_4 D domain in the C-terminal direction (row 4, $\beta_{4b}\Delta C(\alpha_{1B})$). Whatever the cause, it is likely to be different for α_{1B} complexes containing $\beta_{4a}\Delta C$ versus $\beta_{4b}\Delta C$. Adding back the C terminus to $\beta_{4a}\Delta C$ has no effect on α_{1B} mode A_2I_2 (row 5), whereas addition of the C terminus to $\beta_{4b}\Delta C$ causes a shift to mode A_1I_1 (row 6). Row 4 also shows that $\beta_{4b}\Delta C$ causes an α_{1A} subunit mode change that is limited to activation (A_2I_1). This was the one instance in our experiments in which regulation of activation and inactivation were separable functions. The addition of the C terminus to $\beta_{4a}\Delta C$ shifts α_{1A} to mode A_2I_2 (row 5), which again is likely the result of a β_4 C-terminal binding event. The addition of the C terminus to $\beta_{4b}\Delta C$ creates a distinct α_{1A} mode, A_1I_3, characterized by steep activation and inactivation.

In conclusion, our results add to the developing picture of the intracellular domains surrounding the Ca^{2+} channel pore being composed of modular "hot spots" for channel regulation by β-subunits, protein kinases, G-proteins, syntaxin, and calmodulin (for review, see Walker and DeWaard, 1998; Levitan, 1999). Our future experiments will be directed toward understanding how interactions between these diverse regulatory components might contribute to the dynamic molecular events giving rise to synaptic plasticity.

REFERENCES

Berrou L, Bernatchez G, Parent L (2001) Molecular determinants of inactivation within the I-II linker of α_{1E} (CaV2.3) calcium channels. Biophys J 215–228.

Birnbaumer L, Qin N, Olcese R, Tareilus E, Platano D, Costantin J, Stefani E (1998) Structures and functions of calcium channel β subunits. J Bioenerg Biomembr 30:357–375.

Bourinet E, Soong TW, Sutton K, Slaymaker S, Mathews E, Monteil A, Zamponi GW, Nargeot J, Snutch TP (1999) Splicing of α_{1A} subunit gene generates phenotypic variants of P- and Q-type calcium channels. Nat Neurosci 2:407–415.

Cens T, Restituito S, Charnet P (1999) Regulation of Ca-sensitive inactivation of a L-type Ca^{2+} channel by specific domains of β subunits. FEBS Lett 450:17–22.

De Waard M, Campbell KP (1995) Subunit regulation of the neuronal α_{1A} Ca^{2+} channel expressed in *Xenopus* oocytes. J Physiol (Lond) 485:619–634.

Ellinor PT, Zhang JF, Randall AD, Zhou M, Schwarz TL, Tsien RW, Horne WA (1993) Functional expression of a rapidly inactivating neuronal calcium channel. Nature 363:455–458.

Fanning AS, Anderson JM (1999) Protein modules as organizers of membrane structure. Curr Opin Cell Biol 11:432–439.

Hanlon MR, Berrow NS, Dolphin AC, Wallace BA (1999) Modelling of a voltage-dependent Ca^{2+} channel β subunit as a basis for understanding its functional properties. FEBS Lett 445:366–370.

Herlitze S, Hockerman GH, Scheuer T, Catterall WA (1997) Molecular determinants of inactivation and G protein modulation in the intracellular loop connecting domains I and II of the calcium channel α_{1A} subunit. Proc Natl Acad Sci USA 94:1512–1516.

Horne WA, Ellinor PT, Inman I, Zhou M, Tsien RW, Schwarz TL (1993) Molecular diversity of Ca^{2+} channel α_1 subunits from the marine ray *Discopyge ommata*. Proc Natl Acad Sci USA 90:3787–3791.

Jones LP, Wei SK, Yue DT (1998) Mechanism of auxiliary subunit modulation of neuronal α_{1E} calcium channels. J Gen Physiol 112:125–143.

Kozak M (1991) An analysis of vertebrate mRNA sequences: intimations of translational control. J Cell Biol 115:887–903.

Krovetz HS, Helton TD, Crews AL, Horne WA (2000) C- terminal alternative splicing changes the gating properties of a human spinal cord calcium channel α_{1A} subunit. J Neurosci 20:7564–7570.

Lacerda AE, Kim HS, Ruth P, Perez-Reyes E, Flockerzi V, Hofmann F, Birnbaumer L, Brown AM (1991) Normalization of current kinetics by interaction between the α_1 and β subunits of the skeletal muscle dihydropyridine-sensitive Ca^{2+} channel. Nature 352:527–530.

Letts VA, Felix R, Biddlecome GH, Arikkath J, Mahaffey CL, Valenzuela A, Bartlett 2nd FS, Mori Y, Campbell KP, Frankel WN (1998) The mouse stargazer gene encodes a neuronal Ca^{2+} channel γ subunit. Nat Genet 19:340–347.

Levitan IB (1999) It is calmodulin after all! Mediator of the calcium modulation of multiple ion channels. Neuron 22:645–648.

Liu H, De Waard M, Scott VE, Gurnett CA, Lennon VA, Campbell KP (1996) Identification of three subunits of the high affinity omega-conotoxin MVIIC-sensitive Ca^{2+} channel. J Biol Chem 271:13804–13810.

Mikami A, Imoto K, Tanabe T, Niidome T, Mori Y, Takeshima H, Narumiya S, Numa S (1989) Primary structure and functional expression of the cardiac dihydropyridine-sensitive calcium channel. Nature 340:230–233.

Mori Y, Friedrich T, Kim MS, Mikami A, Nakai J, Ruth P, Bosse E, Hofmann F, Flockerzi V, Furuichi T, Mikoshiba K, Imoto K, Tanabe T, Numa S (1991) Primary structure and functional expression from complementary DNA of a brain calcium channel. Nature 350:398–402.

Olcese R, Qin N, Schneider T, Neely A, Wei X, Stefani E, Birnbaumer L (1994) The amino terminus of a calcium channel β subunit sets rates of channel inactivation independently of the subunit's effect on activation. Neuron 13:1433–1438.

Pan JQ, Lipscombe D (2000) Alternative splicing in the cytoplasmic II-III loop of the N-type Ca^{2+} channel α_{1B} subunit: functional differences are β subunit-specific. J Neurosci 20:4769–4775.

Pragnell M, De Waard M, Mori Y, Tanabe T, Snutch TP, Campbell KP (1994) Calcium channel β-subunit binds to a conserved motif in the I-II cytoplasmic linker of the α_1-subunit. Nature 368:67–70.

Qin N, Olcese R, Zhou J, Cabello OA, Birnbaumer L, Stefani E (1996) Identification of a second region of the β subunit involved in regulation of calcium channel inactivation. Am J Physiol 271:C1539–1545.

Scott VE, De Waard M, Liu H, Gurnett CA, Venzke DP, Lennon VA, Campbell KP (1996) β subunit heterogeneity in N-type Ca^{2+} channels. J Biol Chem 271:3207–3212.

Singer D, Biel M, Lotan I, Flockerzi V, Hofmann F, Dascal N (1991) The roles of the subunits in the function of the calcium channel. Science 253:1553–1557.

Stotz SC, Hamid J, Spaetgens RL, Jarvis SE, Zamponi GW (2000) Fast inactivation of voltage-dependent calcium channels. A hinged-lid mechanism? J Biol Chem 275:24575–24582.

Takahashi T, Momiyama A (1993) Different types of calcium channels mediate central synaptic transmission. Nature 366:156–158.

Tareilus E, Roux M, Qin N, Olcese R, Zhou J, Stefani E, Birnbaumer L (1997) A *Xenopus* oocyte β subunit: evidence for a role in the assembly/expression of voltage-gated calcium channels that is separate from its role as a regulatory subunit. Proc Natl Acad Sci USA 94:1703–1708.

Turner TJ, Adams ME, Dunlap K (1992) Calcium channels coupled to glutamate release identified by omega-Aga-IVA. Science 258:310–313.

Walker D, De Waard M (1998) Subunit interaction sites in voltage-dependent Ca^{2+} channels: role in channel function. Trends Neurosci 21:148–154.

Walker D, Bichet D, Campbell KP, De Waard M (1998) A β_4 isoform-specific interaction site in the carboxyl-terminal region of the voltage-dependent Ca^{2+} channel α_{1A} subunit. J Biol Chem 273:2361–2367.

Walker D, Bichet D, Geib S, Mori E, Cornet V, Snutch TP, Mori Y, De Waard M (1999) A new β subtype-specific interaction in α_{1A} subunit controls P/Q-type Ca^{2+} channel activation. J Biol Chem 274:12383–12390.

Westenbroek RE, Ahlijanian MK, Catterall WA (1990) Clustering of L-type Ca^{2+} channels at the base of major dendrites in hippocampal pyramidal neurons. Nature 347:281–284.

Westenbroek RE, Hoskins L, Catterall WA (1998) Localization of Ca^{2+} channel subtypes on rat spinal motor neurons, interneurons, and nerve terminals. J Neurosci 18:6319–6330.

Wheeler DB, Randall A, Tsien RW (1994) Roles of N-type and Q-type Ca^{2+} channels in supporting hippocampal synaptic transmission. Science 264:107–111.

Wittemann S, Mark MD, Rettig J, Herlitze S (2000) Synaptic localization and presynaptic function of calcium channel β_4 subunits in cultured hippocampal neurons. J Biol Chem 275:37807–37814.

Wu LG, Westenbroek RE, Borst JG, Catterall WA, Sakmann B (1999) Calcium channel types with distinct presynaptic localization couple differentially to release in single calyx-type synapses. J Neurosci 19:726–736.

Zhang JF, Ellinor PT, Aldrich RW, Tsien RW (1994) Molecular determinants of voltage-dependent inactivation in calcium channels. Nature 372:97–100.